The "Electron-Root" Feature in the WENDELSTEIN-7-AS Stellarator with ECRH in O1-Mode Compared to X2-Mode

M. Romé[†], C.D. Beidler, H. Maaßberg,

N.B. Marushchenko, Yu.A. Turkin, and the W7-AS Team

Max-Planck Institut für Plasmaphysik,

EURATOM Association, D-85748 Garching, Germany

[†] *I.N.F.N., Dipartimento di Fisica, Università degli Studi, I-20133 Milano, Italy*

(Dated: December 16, 2005)

Abstract

At the W7-AS stellarator, the neoclassical "electron-root" was found in discharges with Electron Cyclotron Resonance Heating (ECRH) in both O1- and X2-mode. The electron heat diffusivity estimated from the power balance is compared with neoclassical predictions with the radial electric field, E_r, from the ambipolarity condition taken into account. Strongly positive E_r values significantly reducing the electron neoclassical transport coefficients are found in the central region with highly peaked T_e-profiles. Furthermore, the "electron-root" feature in the ECE time-traces is analysed in the phase when the ECRH is switched off.

The power deposition in phase space is analysed with ray-tracing and bounce-averaged Fokker-Planck calculations. For the O1-mode, the power is almost completely absorbed by passing electrons. These findings are different from the previous X2 results [1] for the magnetic configuration with a significant fraction of ripple-trapped electrons in the ECRH launching plane. For this X2 scenarios, fast "convective" contributions to the radial fluxes had been identified. For the O1-scenarios, a purely "diffusive" neoclassical modelling of the power threshold for obtaining the "electron-root" in the different magnetic configurations is described based on the concept of the "effective helical ripple". Finally, a simulation of the ECRH switch-off by solving the time-dependent electron energy balance is performed. The results show that the "electron-root" feature at W7-AS is consistent with the neoclassical predictions.

I. INTRODUCTION

The neoclassical "electron-root" (e-root) feature (following the "tokamak fashion" also called "electron" and "neoclassical internal transport barrier", eITB and nITB, respectively) has been observed in the main stellarator experiments, namely in CHS [2, 3], LHD [4, 5], TJ-II [6, 7] and W7-AS [1, 8]. This feature is obtained only for electron cyclotron resonance heating (ECRH) with central deposition and is characterised by a centrally peaked electron temperature profile in combination with strongly positive radial electric fields, E_r. At very low densities the range of $E_r > 0$ can even extend over the whole plasma radius, see e.g. [9, 10]. Within the e-root region, the density and the ion temperature profiles are rather flat, and, consequently, a strong $E_r > 0$ is required to reduce the electron fluxes and to ensure ambipolarity [11, 12]. This neoclassical "electron-root" only exists in the stellarator long-mean-free-path (*lmfp*) regime and is characterised by the transition from the (unfavourable) $\frac{1}{\nu}$-regime for very small E_r to the $\sqrt{\nu}$- or ν-regime for stronger E_r (with significantly reduced heat transport). The $E \times B$ rotation can significantly reduce the radial deviation of the drift surfaces of ripple-trapped electrons from the flux surfaces thus improving the confinement; see e.g. Ref. [13].

The neoclassical nature of this e-root feature is reasonably well confirmed in stellarator experiments [1] with quite different signatures than for tokamak ITBs; see [14] for the comparison in LHD and in JT-60U. In tokamaks, the strong E_r at the barrier position, i.e. the sheared $E \times B$ flow, reduces the anomalous part of the transport (driven by ITG and TEM turbulence, ETG being a small-scale turbulence is not affected by the $E \times B$ flow), in particular the ion thermal diffusivity, down to the neoclassical level; see e.g. the reviews [15, 16] for more details. An international collaboration on an inter-machine comparison and analysis of the e-root feature in the stellarators mentioned above has recently been initiated [17].

In the early phase, W7-AS had been equipped with up to four 70 GHz gyrotrons with up to 200 kW each. The "standard" operation at $B = 2.5$ T with 70 GHz ECRH in *1st* harmonic O-mode (O1) and later operation with 140 GHz in *2nd* harmonic X-mode (X2) allows the analysis of the different absorption in phase space and of its impact on the e-root feature. Unfortunately, the e-root was not recognised in this early operation phase [18], but recently some main e-root signatures could be identified using the experience of the findings with 140 GHz X2-mode. Furthermore, in that early phase of W7-AS operation, the vertical ruby-laser chord of the old Thomson diagnostic was slightly misalligned (the effect was strengthened by the Shafranov shift) and missed the central e-

root region. The ECE diagnostic with the horizontal chord, however, found (in some cases) much higher central T_e values compared to the Thomson data. Later on, this discrepancy was resolved by shifting the plasma with a vertical field over the laser chord. In addition, no E_r data from the active CXRS diagnostic were available in this early experimental phase.

At the W7-AS stellarator, the e-root feature was first observed and interpreted by the neoclassical effect in 1996. In this later phase of W7-AS operation, the ECRH system had already been upgraded to three 140 GHz gyrotrons, each with about 500 kW power. The densities in these experiments ranged from $1.5 \cdot 10^{19}$ to $7 \cdot 10^{19}$ m^{-3} leading to much lower T_i compared to T_e for the purely ECR heated discharges. Measured using the active CXRS diagnostic [8], strongly positive E_r values were found only in discharges with a highly peaked T_e-profile and were consistent with the neoclassical E_r from the ambipolarity condition. Additionally, the electron thermal diffusivity from the power balance outside of the e-root region (up to $2/3$ of the plasma radius) was also in good agreement with the neoclassical prediction.

The main criteria for the neoclassical e-root feature are briefly summarised in the following; for more details see Ref. [1]. The central T_e profile must be highly peaked. In this region, strongly positive radial electric fields reduce the neoclassical electron heat flux (unfortunately, E_r measurements for the O1-discharges described in this paper are missing). The experimental electron heat diffusivity, χ_e, must be much smaller than the neoclassical prediction for the $\frac{1}{\nu}$-regime, i.e. for $E_r = 0$; this is analysed in Sec. II A. Thresholds in density and heating power must exist for establishing the e-root feature; these thresholds depend on the magnetic configuration. For example, in Ref. [1] it was concluded that the fraction of ripple-trapped electrons in the launching plane leading to "convective" losses for scenarios with ECRH in X2-mode is an important parameter. Equivalent discharges in O1-mode for two magnetic configurations with a different fraction of ripple-trapped electrons are analysed in Sec. II A which motivated the Fokker-Planck simulations of Sec. III.

Since the e-root feature is based on a bifurcation mechanism (several roots of the neoclassical ambipolarity condition), spontaneous and triggered transitions can appear close to the threshold (the "electric pulsations" in [2]). Spontaneous transitions are not found for the discharges described here, e.g. a detailed B-scan (as done for the X2-scenarios) is missing. Switching-off the ECRH leads to a fast decay of the e-root feature which may be identified by the central E_r time traces obtained from the heavy ion beam probe (HIBP) diagnostic [2] (not available at W7-AS). As an alternative, this decay can be identified from the central T_e time traces measured by the ECE

diagnostic; these results are described in Sec. II B.

The main findings for ECRH in O1-mode are described in Section II and will be compared to the results with X2-mode. For the fairly high T_e with central deposition, the single-pass absorptions for O1- and X2-mode (both launched from the low-field side) are comparable (more than 90% and nearly 100%, respectively) in the linear approach being in the ray-tracing calculations [19, 20]. For these scenarios with highly localised central power deposition (toroidally averaged power densities up to 50 W/cm^3), however, a significant quasi-linear degradation of the absorption due to the flattening of the electron distribution function close to the (relativistic) phase-space resonance might be expected. Section III describes the ray-tracing calculations and Fokker-Planck simulations [21, 22] for ECRH both in O1- and in X2-mode. Based on the experience with X2-scenarios as well as with high-power ECCD [23], the following aspects are of particular interest: the quasi-linear degradation of the single-pass absorption in O1-mode, the fraction of power absorbed by the ripple-trapped electrons in the ECRH-launching plane, and, finally, the impact of the "Ohkawa effect" [24], i.e. the trapping of barely passing electrons due to the wave absorption. Furthermore, a purely neoclassical analysis of the power threshold for the e-root feature and a time-dependent simulation of the ECRH switch-off are described. Finally, conclusions are given in Section IV.

II. EXPERIMENTAL RESULTS FOR O1-MODE

A. Stationary ECRH Power and Density Scans

Figure 1 shows n_e- and T_e-profiles for two ECRH power scans with 2 to 4 gyrotrons at low and high rotational transform, ι. In the scan with the edge value $\iota_a = 0.52$, the T_e from Thomson scattering and from the ECE agree quite well. The ECE channel on the low-field-side at 138.7 GHz (X2-mode) corresponding to $r \simeq 3$ cm is sometimes disturbed by about 10 to 20% from one gyrotron as can be seen at the switch-off. In the profile fits, this channel (leading to an overestimate of T_e) was excluded when a disturbance could be identified. In the high-ι power scan, the central peaking of the T_e-profile is missing, although the situation might be marginal at 690 kW.

In the low-ι power scan in Figure 1, the T_e-profiles are highly peaked for 470 kW and 650 kW. The neoclassical transport analysis shows that the power threshold for establishing the e-root feature is between 340 kW and 470 kW (see below). In these discharges, the central part of the profiles was not covered by the Thomson diagnostic since the vertical laser chord (positioned in the vertically

elongated plane) was slightly misalligned as was identified later on. In particular at low ι, the Shafranov shift of the magnetic axis becomes significant due to the peaked pressure profile and the toroidal current density profile lowering the central ι [23]. In these net-current-free discharges, the bootstrap current is feed-back controlled by an inductive current ($j_{\rm ind} < 0$) which is also strongly peaked. In principle, all these pressure and current density effects might be included in the VMEC equilibrium [25] calculations for an improved mapping of the positions along the laser chord to the effective radius. In this early operational phase, however, a rather simplified mapping of the experimental data to magnetic coordinates with only pressure effects taken into account was applied. Consequently, an additional "correction" of the central radii of the n_e and T_e from Thomson scattering is applied. Except for of the low n_e-discharge shown in Figs. 4 and 5, the central data from Thomson scattering are mapped to radii corresponding to the T_e-fit to the ECE data in the central region. For this low n_e discharge of Figs. 4 and 5, however, an additional fit of the magnetic axis position improved the mapping of the Thomson scattering data in the central region.

The neoclassical transport in both the low-ι and high-ι configurations is roughly equivalent in the central part. The "effective helical ripple", $\epsilon_{\rm eff}$ (defined by the same transport in the $\frac{1}{\nu}$-regime, i.e. for $E_r = 0$, as in a "classical" stellarator with helical ripple $\epsilon_h = \epsilon_{\rm eff}$) is between 1 and 2% for $r \leq 6$ cm; see Sec. III B. However, the fraction of ripple-trapped electrons in the ECRH launching-plane is quite different as is shown in Fig. 2. Direct power absorption by these ripple-trapped electrons (this is the case for X2-mode) can lead to significant "convective" particle and heat fluxes [26] in addition to the "diffusive" neoclassical ones.

Figure 3 shows the results of the neoclassical transport analysis of the low-ι discharge with 650 kW ECRH power of Fig. 1 (on the right). The neoclassical transport coefficients for the rather complex W7-AS configurations are obtained with energy convolution from the database of mono-energetic transport coefficients calculated by the DKES code [27, 28]; see Ref. [18] for more details. Within the range of the highly peaked T_e-profile, only the "electron-root" with strongly positive E_r is obtained from the ambipolarity of the neoclassical particle fluxes (by root-finding). For these E_r, the neoclassical heat diffusivity is strongly reduced compared to the case with $E_r = 0$ and is in good agreement with the "experimental" heat diffusivity. The latter is obtained by integrating the electron power balance and fitting to the measured T_e data; see Ref. [18] for more details. The important point in this context, namely that the experimental heat diffusivity is much less than the neoclassical prediction with $E_r = 0$, is obvious for this low-ι discharge. For the equivalent high-ι

discharge with 690 kW ECRH, however, the situation is different (the heat transport analysis and the comparison with the neoclassical prediction are not shown). Although an "electron-root" is also obtained for $r \leq 3$ cm, the experimental heat diffusivity agrees with the neoclassical one for $E_r = 0$, i.e. improved heat confinement is not indicated in the center.

A density scan of low-ι discharges with 3 and 4 gyrotrons is shown in Figure 4. The neoclassical transport analysis for the low-n_e discharge is given in Figure 5. Equivalent to the high-n_e discharge of Fig. 3, a pronounced "electron-root" E_r is obtained for $r \leq 7$ cm. Only for $r \leq 5$ cm, the neoclassical $\frac{1}{\nu}$-heat diffusivity with $E_r = 0$ (dotted line) exceeds significantly the experimental one supporting the e-root interpretation also for this low-n_e discharge. In this density scan for ECRH in O1-mode, the T_e outside of the e-root region depends strongly on density (and also limiter radius). This finding is different to the n_e-scan with 1.2 MW in X2-mode (see Fig. 3 on the left in Ref. [1]) where T_e outside of the e-root region was roughly independent of n_e thus directly confirming the $\frac{1}{\nu}$-transport. Moreover, the experimental χ_e was in reasonable agreement with the neoclassical heat diffusivity up to about $\frac{2}{3}$ of the plasma radius due to the higher T_e for these X2-scenarios. In the early phase of W7-AS with 70 GHz ECRH (O1-mode), movable titanium carbide limiters were installed and no boronisation was applied leading to higher radiation losses compared to the X2-scenarios in the later phase with boronisation and carbon limiters on the inner wall; see [29]. Nevertheless, the discrepancy of the experimental and the neoclassical electron heat diffusivity for these O1-scenarios outside of the e-root region is not yet understood.

The best agreement of the experimental χ_e and the neoclassical heat diffusivity within the e-root region is found for high density and low ECRH power (but above the threshold); see e.g. Fig. 3. With smaller n_e, χ_e significantly exceeds the neoclassical prediction for the e-root; see Fig. 5 as the "worst" case. This tendency supports the hypothesis that additional "diffusive" fluxes being related to the (ECRH driven) deviation of the electron distribution function from the Maxwellian might be important; see Sec. III A.

B. Switching-off the ECRH

Figure 6 shows some time traces of the ECE electron temperature in channels within the e-root region and outside it. The discharge with O1-mode (on the left) is comparable to the X2-mode discharge in Ref. [1] with respect to density, ECRH power and magnetic configuration. The decay time of the central ECE channels, however, is slower with about 3.1 ms compared to the X2-

scenario with about 1.5 ms immediately after the switch-off. For the O1-mode discharges, the decay time in the ECE-channels outside of the e-root region is about 7.5 ms which is equivalent to those of the central channels about 1 ms after the ECRH is switched off. For the low-n_e discharge (on the right), the decay time is only slightly shorter (2.8 ms), but again slower compared to the X2 reference discharge. Thus, the e-root feature for ECRH in O1-mode is also confirmed by the faster decay immediately after the switch-off, but a clear difference to the X2-scenarios is found.
For ECRH in X2-mode in the low-ι configuration, a significant fraction of the power is absorbed by the electrons trapped within the ripple in the launching plane; see Fig. 2. These ECRH-driven deviations in the distribution function from the Maxwellian represent a "convective" particle and energy flux [26] adding to the neoclassical one. For the O1-mode, however, the situation is completely different: only a very small fraction of the power is absorbed by trapped electrons; see Sec. III A. For this scenario, pitch-angle scattering is responsible for the energy flux to the ripple-trapped electrons which dominate the transport in the *lmfp*-regime (at least for moderate E_r). In this sense, the additional fluxes driven by the ECRH in O1-mode are smaller than those for X2-mode. In addition, the time-scales are different: for the O1-scenario, the collisional time-scale adds to the radial ∇B-drift time for the X2-mode. Consequently, the radial polarization current density (eq. 4 as well as eq. 10 in Ref. [1]) related to the ECRH switch-off is significantly smaller for O1-mode leading to a slower decay of the e-root feature.

III. MODELLING AND DISCUSSIONS

The electron distribution function can be significantly perturbed by the local ECRH deposition. This deviation from the Maxwellian at slightly suprathermal energies ($v > v_{th}$) leads to particle and energy fluxes exceeding the neoclassical ones which in the traditional approach are driven only by the gradients of the Maxwellian. In particular for the O1-scenarios, where the direct power absorption by ripple-trapped particles is negligible for both magnetic configurations, a purely neoclassical modelling of the e-root feature is performed; this is described in Sec. III B.

A. Effects of the ECRH on the Electron Distribution Function

The deviation of the electron distribution function from the Maxwellian is estimated by means of a bounce-averaged Fokker-Planck code [21] with a quasi-linear diffusion term describing the ECR

power deposition. The flux-surface-averaged quasi-linear diffusion coefficient, $D_{\perp\perp}(r, v_\parallel, v_\perp)$, is obtained from ray-tracing calculations in the framework of linear theory. The 3D Hamiltonian ray-tracing code integrates the radiative transfer equation using the cold plasma dispersion relation and with absorption and emission coefficients computed in the weakly relativistic limit. The "local" quasi-linear diffusion coefficient

$$D_{\perp\perp} = \frac{\pi e^2}{2m^2 v_\perp^2} \left|\Theta_\ell\right|^2 \delta(\omega - k_\parallel v_\parallel - \frac{\ell\omega_c}{\gamma}) \tag{1}$$

is evaluated for each ray and averaged for all rays over a narrow radial shell. Here, $k_\parallel$ is the parallel wave vector component ($\simeq 0$ for perpendicular launching), ω_c/γ the relativistic cyclotron frequency, ℓ the wave harmonic, and Θ_ℓ the polarization term (for small $k_\parallel$),

$$\Theta_{O1} \simeq v_\parallel E_\parallel J_1(k_\perp \rho_e) \qquad \text{and} \qquad \Theta_{X2} \simeq v_\perp E_- J_1(k_\perp \rho_e),$$

with E_- ($E_\parallel$) the left-polarised (parallel) electric field component, J_1 the Bessel function of the first kind, $k_\perp$ the normal wave vector component, and $\rho_e = v_\perp/\omega_c$ the electron gyro-radius. Due to the variation of B (i.e. ω_c) within the absorption region (the EC-beam width is about 5 cm), a fairly strong broadening of the averaged $D_{\perp\perp}$ is obtained for the highly peaked central deposition (spectral broadening effects due to the finite beam width being less important).

Both O1- and X2-mode absorptions have an equivalent scaling with temperature (the optical depth $\tau \propto nT_e$), but the O1-mode has less absorption efficiency for perpendicular injection. For the fairly high central T_e in the analysed discharges, however, the single path absorption is very close to 100% for both cases in the linear approach. Furthermore, with increasing T_e the absorption in velocity space is shifted into the thermal bulk, and quasi-linear degradation effects become less important (for the analysis at lower T_e, see [22]). Bounce-averaged Fokker-Planck simulations of the electron distribution function, f, are applied to confirm these conclusions from the linear approach. In these time-dependent simulations, the power source from the quasi-linear diffusion term with the averaged diffusion coefficient calculated from ray-tracing must be balanced by a power sink, $S \cdot f$, simulating the radial energy transport,

$$\frac{\partial}{\partial t}\langle f\rangle \simeq \langle C(f)\rangle + \Big\langle \frac{1}{v_\perp}\frac{\partial}{\partial v_\perp} v_\perp D_{\perp\perp} \frac{\partial}{\partial v_\perp} f \Big\rangle + \langle S \cdot f\rangle \tag{2}$$

where $\langle ... \rangle$ indicates bounce-averaging; see Ref. [21] for more details. Note that a more accurate transport modelling for stellarators demands a (bounce-averaged) Fokker-Planck treatment in 4D phase space; such solvers are not yet available. In principle, Monte Carlo techniques (see e.g.

Refs. [26, 30]) might be used for estimating the ECRH-driven additional fluxes. A "traditional" MC technique, however, is very inefficient for ECRH simulations since the phase-space volume with wave-particle interactions (also in the quasi-linear approach) is very small. Consequently, the transport modelling by simple sink terms is a rough, but reasonable approximation in the Fokker-Planck simulations.

Equivalent to the neoclassical transport in the $\frac{1}{\nu}$-regime, only the radial component of the ∇B-drift of ripple-trapped electrons contributes to the particle and power loss. Power absorption by passing electrons must be compensated by the sink term acting only on the ripple-trapped electrons. The deviation of the distribution function from the Maxwellian in the passing particle domain is linked to the distribution function of the ripple-trapped electrons by pitch-angle scattering. However, this represents a "diffusive" contribution to the particle and energy flux similar to the neoclassical one: inward- and outward drifting electrons balance each other. Equivalent to the neoclassical expansion where the (total) derivative of the Maxwellian leads to the "thermodynamic forces", i.e. the gradients of density, temperature and electric potential, the radial gradient of the absorbed power density drives such an additional "diffusive" flux.

For balancing the power absorbed by passing particles, the "diffusive" sink model, S^d, is used whereas the "convective" one, S^c, is used for the power absorbed by the trapped particles

$$S^d \cdot f \propto (\underline{v}_{\nabla B}|_r)^2 \, \mathcal{H}(p^2_{\mathrm{lc},\,d} - p^2)\, f \qquad \text{and} \qquad S^c \cdot f \propto \underline{v}_{\nabla B}|_r \, \mathcal{H}(p^2_{\mathrm{lc},\,c} - p^2)\, f \tag{3}$$

where $\mathcal{H}$ is the step function, and p_{lc} the pitch ($p = v_{\|}/v$) of the loss-cone. For the "convective" sink modelling, a simple geometrical definition of the loss-cone size with respect to the ECRH launching is appropriate: $p^2_{\mathrm{lc},\,c} = 1 - B_{\mathrm{res}}/B_{\max}$ where B_{res} is the resonant value of the magnetic field at the ECRH launching position, and $B_{\max}$ is its maximum value at the axis (see Fig. 2). In general, a different loss-cone size should be used for the "diffusive" modelling. For a "classical" stellarator configuration, $p^2_{\mathrm{lc},\,d} = 2\epsilon_h$ holds. The generalisation for optimized configurations corresponding to the neoclassical ϵ_{eff}, however, might be misleading, since the drift-optimisation reduces $\underline{v}_{\nabla B}|_r$, but not the fraction of particles being involved in the "diffusive" loss process. Consequently, also a "geometrical" ripple might be used: $p^2_{\mathrm{lc},\,d} = 1 - B_{\min}/B_{\max}$ with $B_{\min}$ being the minimum of B on the flux surface. In principle, some freedom exists in defining $p_{\mathrm{lc},\,d}$. In the low-ι "standard" configuration of Fig. 2, for example, $p_{\mathrm{lc},\,d} = p_{\mathrm{lc},\,c}$ is a quite reasonable estimate since also the neoclassical ϵ_{eff} is dominated by the local ripple in the ECRH launching plane with the fairly strong (local) toroidal curvature.

Since both sink terms describe also the loss of particles, a simple $\dot{n}$-source model ($S^n \propto f$) is used for compensation. The three free parameters of these sink and source terms are adjusted to fulfil the energy and particle balances in the time-dependent Fokker-Planck simulations. In particular for the energy balance, the power absorbed by the passing particles and by the ripple-trapped particles is used for adjusting the "diffusive" and the "convective" sink strength, respectively (separated energy balance). This time-dependent process is executed in such a way that the electron temperature is conserved (which is defined by the pitch-angle integrated slope of the distribution function at very low energies). The Fokker-Planck calculations are performed up to stationary conditions.

Figure 7 shows the electron distribution function both for O1-mode and X2-mode (as reference) at the (toroidal) ECRH-position close to the axis ($r = 0.75$ cm) for the low-ι "standard" configuration with the larger loss-cone; comp. Fig. 2. The simulations are performed for $n_e = 3 \cdot 10^{19}$ m^{-3}, $T_e \simeq 3$ keV and 30 MW/m^3 power density (from the linear approach) corresponding to about 500 kW ECRH with central deposition. For both scenarios, a moderate quasi-linear degradation effect due to the flattening of the distribution function in the absorption zone is found (0.8 and 0.7 for O1 and X2, respectively). In particular for the X2-mode, the distribution function strongly flattens and the quasi-linear degradation for the trapped electrons is much stronger than the one for passing electrons. For the O1-mode, the "Ohkawa effect" (trapping of passing particles due to the quasi-linear diffusion) is found to be negligible.

These results indicate that kinetic effects directly related to the ECRH are much smaller for the O1- compared to the X2-scenario. For the low-ι configuration with a maximum of B in the ECRH launching plane as described in Ref. [1], the X2- is rather comparable to the O1-scenario of Fig. 7 with the minimum of B. Consequently, a neoclassical modelling without significant ECRH-driven "convective" particle fluxes turns out to be a reasonable approximation for the e-root feature in the O1-mode (also for the X2-mode in the "maximum-B" configuration; comp. Fig. 2).

B. Neoclassical Modelling

In the neoclassical $\frac{1}{\nu}$-regime, both the particle and heat fluxes scale with $\epsilon_{\text{eff}}^{3/2}$ (ϵ_{eff} being the effective helical ripple; see Sec. II A). In particular on axis, $\epsilon_{\text{eff}}(0) \simeq 0.8\%$ both for the high-ι "standard" configuration (see Fig. 2) and for the "maximum-B" configuration of Ref. [1], and $\epsilon_{\text{eff}}(0) \simeq 1.1\%$ for the low-ι "standard" configuration. Consequently, the $\frac{1}{\nu}$-transport is by a factor

of about 1.6 larger in the low-ι "standard" configuration where the lowest threshold for the e-root feature in the power scans compared to the other configurations is obtained.

Two scenarios are found in the transport analysis: i) The experimental χ_e obtained from the electron power balance analysis outside of the e-root region (with small $E_r > 0$) is consistent with the neoclassical heat diffusivity for the "ion-root", i.e. roughly with the $\frac{1}{\nu}$-diffusion coefficient. Then, the bifurcation to the e-root feature is described completely within the neoclassical ambipolarity of the particle fluxes in the radial range with multiple roots (from root-finding), and the position of the transition is obtained from the (stationary) diffusion equation for E_r (comp. eq. 4). ii) The electron $\frac{1}{\nu}$-heat diffusivity reaches χ_e (which is much larger than the neoclassical one at outer radii for the O1-scenarios described here) only at the transition position; see Fig. 3. Without bifurcation to the e-root, the central T_e-profile must flatten to be consistent with the energy balance, otherwise the established e-root with the strong reduction of the heat diffusivity allows for the peaking of the T_e-profile. In parallel, also the neoclassical particle fluxes must fulfil the particle balance with the ionisation of neutrals being the particle source (neither NBI nor pellet injection was used in these discharges). Furthermore, the density profiles are also determined by the ion transport which violates the "traditional" neoclassical ordering given the strong E_r of the e-root; see [1] for more details. From the experimental point of view, however, no flattening of the central T_e-profile was observed indicating that the bifurcation to the e-root with the improved central confinement is preferred.

Depending on heating power and density, the bifurcation to the e-root appears at an experimental heat diffusivity of $0.4 \leq \chi_e \leq 3$ m^2/s, this value is lowest for low heating power and high density. This χ_e-level must be compared with the neoclassical value in the $\frac{1}{\nu}$-regime, i.e. for configurations with larger ϵ_{eff} the bifurcation to the e-root appears at lower heating power for equivalent temperatures. From this purely neoclassical interpretation, the power threshold for the e-root feature scales with $\epsilon_{\text{eff}}^{-3/2}$. For example, the power threshold in the low-ι "standard" configuration is between 340 kW and 470 kW and in the high-ι configuration more than 690 kW (comp. Fig. 1 with (slightly) different densities and plasma radii). The ratio of these thresholds is roughly consistent with the ϵ_{eff}-scaling in the $\frac{1}{\nu}$-regime. Furthermore, the power threshold of the e-root for the X2-scenarios in the "maximum-B" configuration of Ref. [1] is about twice that for the "standard" configuration (both at low ι), for the latter a "convective" flux contribution must be taken into account.

The purely neoclassical transition to the e-root feature depends on heating power, density and on the magnetic configuration. The heating power increases T_e which is the dominant dependence

for the heat diffusivity in the $\frac{1}{\nu}$-regime ($\propto T_e^{7/2}$). On the contrary, the density dependence cancels if the experimental χ_e is consistent with the neoclassical one for the "ion-root"-E_r (i.e. roughly the $\frac{1}{\nu}$-transport); see the density scan in Ref. [1], Fig. 3. The access to the e-root is easier in configurations with higher $\epsilon_{\rm eff}$. This result is also supported by the LHD findings even at the outermost radii [10], where $\epsilon_{\rm eff}$ at the outer radii strongly increases with the magnetic axis radius, $R_{\rm ax}$.

Finally, the purely neoclassical transport modelling is applied to the ECRH switch-off. In these time-dependent simulations, the density profiles are fixed and the energy balance equations both for electrons and for ions are integrated together with the diffusion equation for the ambipolar E_r (see Ref. [31] for more details):

$$M_{\rm eff}\left(1+\frac{\omega_{pi}^2}{\omega_{ci}^2}\right)\varepsilon_0\,\frac{\partial E_r}{\partial t}-\frac{1}{V'}\frac{\partial}{\partial r}\,V'\,D_E\,r\frac{\partial}{\partial r}\,\frac{E_r}{r}=|e|\,(\Gamma_e-Z_i\Gamma_i), \tag{4}$$

Here, $D_E(r)$ approximates a diffusion coefficient for the radial electric field which originates from the poloidal shear viscosity coefficient; see e.g. [18, 32]. V' is the differential volume, Γ_e and Γ_i are the electron and ion particle flux densities, and ω_{pi} (ω_{ci}) is the ion plasma (cyclotron) frequency. The ion inertia is strongly weighted by the ι-profile: the toroidal ion flow driven by the compressible $E\times B$ rotation is equivalent to the Pfirsch-Schlüter current (driven by $\underline{\nabla}p\times\underline{B}/B^2$), and $M_{\rm eff}\simeq 1+(\beta_{10}^*/\iota)^2$ in the limit of a large polidal Mach number (this holds for the e-root); here β_{10}^* is the normalised toroidal curvature which reflects the optimisation due to an "averaged elongation" ($\beta_{10}^*\simeq 0.7$ for W7-AS).

In order to obtain a stationary solution corresponding to the scenario of Fig. 6 (on the left) and Fig. 4 (intermediate n_e), at the outer radii an "anomalous" (stationary) electron heat diffusivity comparable to the experimental χ_e from the power balance is added to the neoclassical transport coefficient obtained with energy convolution from fitting the database of mono-energetic transport coefficients calculated by the DKES code [27, 28]. In this way, the outer T_e-profile is roughly fitted to the experimental one. At the inner radii within the e-root region, which is obtained for stationary conditions in the simulations, the neoclassical fluxes dominate. Since also the stationary transport analysis leads to a χ_e exceeding the purely neoclassical heat diffusivity for the e-root, the ECRH power was reduced to 250 kW (640 kW for the discharge at intermediate density; see Fig. 4) to fit the central T_e-profile. This deviation can be attributed (at least partly) to the additional "diffusive" transport driven by the deviation of the electron distribution from the Maxwellian due to the ECRH power deposition; see Sec. III A. After switching-off the ECRH, both T_e and the

ambipolar E_r decay self-consistently, the latter is damped by the ion inertia term in eq. 4.

Figure 8 shows the simulated $T_e(r,t)$ corresponding to the ECE time-traces of Fig. 6 as well as the $E_r(r,t)$ obtained from eq. 4. The time decay of the T_e-profile in these simulations is in very good agreement with the ECE data shown in Fig. 6: 3.3 ms for the central and 7.7 ms for an outer radius (or at a later phase), the values from ECE are 3.1 ms and 7.5 ms, respectively (see Sec. II B). In this simulation, the ι-profile is assumed for simplicity to be constant leading to a shorter time-scale of the E_r-decay compared to the scenario with the decreased central ι due to the inductive feed-back control of the bootstrap current. The damping of the E_r-decay by the toroidal ion flow is not essential in this simulation, the decay time is equivalent to the T_e one.

An equivalent calculation with increased M_{eff} simulating the strongly decreased central ι leads to a slower E_r decay in the e-root region, however, the decay time of the central T_e is not affected immediately after the ECRH is switched off. Only in the later phase, the T_e decays on a slower time scale. The first simulation indicates, that the e-root feature for these conditions is fairly stable, i.e. it exceeds significantly the power threshold. Only with the significant reduction of the central T_e after about 5 ms, the extension of the e-root shrinks before this feature disappears.

The purely neoclassical modelling of the ECRH switch-off shows very reasonable agreement with the experimental findings, in particular that a "fast" time-scale is lacking unlike the case of the reference discharge with the X2-scenario where "convective" fluxes are indicated [1]; comp. also Fig. 7. All these findings strongly indicate that for the O1-scenarios as well as for the X2-scenario in the "maximum-B" configuration the e-root feature can be described by purely diffusive transport modelling.

IV. SUMMARY AND CONCLUSIONS

The "electron-root" feature is consistent with the neoclassical predictions. In particular, for the ECRH absorption by passing particles, i.e. for the O1-mode in all typical magnetic configurations of W7-AS (also for the X2-mode with the maximum of B in the launching plane [1]), a "diffusive" neoclassical modelling is quite reasonable. For significant X2-mode absorption by ripple-trapped electrons in the launching plane, however, "convective" losses play an important role. In this case, the "convective" fluxes are related to the loss-cone size in the launching plane whereas the "diffusive" fluxes can be related to the "effective helical ripple" describing the averaged transport in the $\frac{1}{\nu}$-regime for small radial electric fields.

Two scenarios are found: i) the experimental heat conductivity is consistent with the neoclassical one in the "ion root" region except at the outermost radii, and ii) the neoclassical heat diffusivity for $E_r \simeq 0$ is much lower than the experimental one outside of the transition position to the e-root feature. In the first case, the transition is simply formulated as a bifurcation between different roots of the ambipolarity of the neoclassical fluxes, the observed spontaneous transitions [1] confirm this neoclassical interpretation. In the second case, the very strong T_e dependence of the neoclassical heat diffusivity ($\propto T_e^{7/2}$) demands either a flattening of the central T_e-profile, which is clearly not observed, or the transition to the e-root in order to reduce the neoclassical transport coefficients and to allow for a highly peaked central T_e-profile.

The transient phase after the ECRH is switched off shows a very fast decay of the e-root T_e-profile only for the case of significant ripple-trapped electron heating which is consistent with the fast "convective" transport contribution adding to the slower "diffusive" one. For the other scenarios without trapped electron heating, a "diffusive" neoclassical modelling, where the E_r-decay is damped by the ion inertia of the Pfirsch-Schlüter-like toroidal flow, is consistent with the experimental decay of the central T_e-profile.

All these findings result in an e-root perspective for W7-X, presently under construction at Greifswald. W7-X is a high-mirror advanced stellarator with a very strong elongation of about 6. For example, the variable "effective helical ripple" on axis with $0 \leq \epsilon_{\text{eff}}(0) \leq 2.5\%$ will allow for an easy access to the e-root feature (at high ϵ_{eff}). Since the ECRH at 140 GHz ($B = 2.5$ T) is launched in X2-mode very close to the maximum of B, the purely "diffusive" neoclassical modelling [31] should be appropriate at least at higher densities. The W7-AS results are in this sense very promising: the e-root feature is obtained at a fairly high density of about $5 \cdot 10^{19}$ m^{-3} and at a moderate ECRH power of about 600 kW. For W7-X, an ECRH power of up to 10 MW will be available, and the cut-off density for X2-mode is $1.25 \cdot 10^{20}$ m^{-3} allowing for better collisional ion heating.

In principle, the e-root feature might also be important for stellarator reactor scenarios if the impurity accumulation cannot be avoided for the "traditional" cases with $E_r < 0$. Note, that the neoclassical temperature screening of the impurities found in tokamaks does not exist in the stellarator *lmfp*-transport regimes. Consequently, the positive E_r of the e-root will push the impurities as well as the helium ash outward. The α-particle heating is roughly equivalent to the ECRH, and the ions are heated only by collisional coupling. An e-root scenario relevant for a stellarator reactor might have lower densities, but higher temperatures. This topic, however, needs further

investigations.

As a last conclusion, the analysis of old experimental data with the present experience and understanding can lead to very surprising findings. After shut-down of an experiment, however, the time and the necessary patience are typically missing for such "data mining".

Acknowledgments

One of the authors (MR) wishes to thank the *Max-Planck-Institut für Plasmaphysik* for their support and hospitality during his stay at IPP-Greifswald. We would also like to thank one of the referees for the lovely formulation "post mortem analysis" to characterise the current work.

---

[1] H. Maaßberg *et al.*, Phys. Plasmas **7**, 295 (2000).

[2] A. Fujisawa *et al.*, Plasma Phys. Control. Fusion **40**, 627 (1998).

[3] T. Minami *et al.*, Nucl. Fusion **44**, 342 (2004).

[4] Y. Takeiri *et al.*, Phys. Plasmas **10**, 1788 (2003).

[5] K. Ida *et al.*, Phys. Plasmas **11**, 2551 (2004).

[6] F. Castejon *et al.*, Nucl. Fusion **42**, 271 (2002).

[7] T. Estrada *et al.*, Plasma Phys. Control. Fusion **46**, 277 (2004).

[8] J. Baldzuhn, M. Kick, H. Maaßberg, and the W7-AS Team, Plasma Phys. Control. Fusion **40**, 967 (1998).

[9] M. Yoshinuma *et al.*, Plasma Phys. Control. Fusion **46**, 1021 (2004).

[10] K. Ida *et al.*, Nucl. Fusion **45**, 391 (2005).

[11] H.E. Mynick and W.N.G. Hitchon, Nucl. Fusion **23**, 1053 (1983).

[12] D.E. Hastings, W.A. Houlberg, and K.C. Shaing, Nucl. Fusion **25**, 445 (1985).

[13] A.A. Galeev and R.Z. Sagdeev, Review of Plasma Physics **7**, 307 (1977).

[14] K. Ida *et al.*, Plasma Phys. Control. Fusion **46**, A45 (2004).

[15] R.C. Wolf, Plasma Phys. Contr. Fusion **45**, R1 (2003).

[16] J.W. Connor and *et al.*, Nucl. Fusion **44**, R1 (2004).

[17] M. Yokoyama *et al.*, *15th International Stellarator Workshop*, Madrid, Spain, 2005, submitted to Fusion Sci. Technol.

[18] H. Maaßberg *et al.*, Phys. Fluids B **5**, 3627 (1993).

[19] U. Gasparino *et al.*, Plasma Phys. Control. Fusion **30**, 283 (1988).

[20] U. Gasparino *et al.*, *Proc. 17th EPS Conf. Contr. Fusion Plasma Phys.*, Amsterdam, 1990, Vol. 14B III, p. 1275.

[21] N.B. Marushchenko, U. Gasparino, H. Maaßberg, and M. Romé, Comp. Phys. Comm. **103**, 145 (1997).

[22] M. Romé *et al.*, Plasma Phys. Control. Fusion **39**, 117 (1997).

[23] H. Maaßberg and M. Romé *et al.*, Plasma Phys. Control. Fusion **47**, 1137 (2005).

[24] V. Erckmann and U. Gasparino, Plasma Phys. Control. Fusion **36**, 1869 (1994).

[25] S.P. Hirshman, W.I. van Rij, and P. Merkel, Comp. Phys. Comm. **43**, 143 (1986).

[26] S. Murakami *et al.*, *Proc. 17th IAEA Fusion Energy Conf.*, Yokohama, Japan, 1998, (IAEA, Vienna, 1999), Vol. 4, p. 1383.

[27] S.P. Hirshman *et al.*, Phys. Fluids **29**, 2951 (1986).

[28] W.I. van Rij and S.P. Hirshman, Phys. Fluids B **1**, 563 (1989).

[29] R. Brakel *et al.*, J. Nucl. Mater. **196-198**, 431 (1992).

[30] S.V. Kasilov, W. Kernbichler, V.V. Nemov, and M.F. Heyn, Phys. Plasmas **9**, 3508 (2002).

[31] Yu.A. Turkin *et al.*, *31th EPS Conf. Plasma Phys. Contr. Fus.*, London 2004, http://epsppd.epfl.ch/London/pdf/P1_198.pdf.

[32] H. Ehmler *et al.*, Nucl. Fusion **43**, L11 (2003).

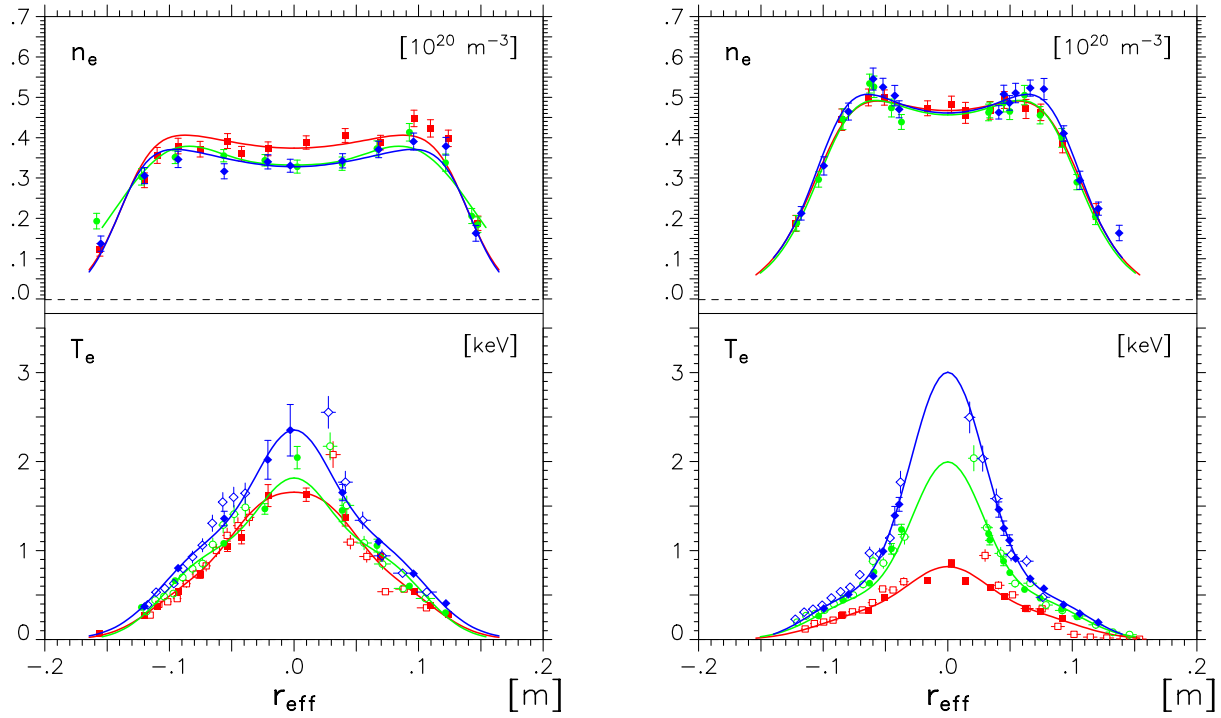

FIG. 1: ECRH power scan (O1-mode): density (on the top) and electron temperature (on the bottom) profiles for $\iota_a = 0.52$ (350 kW, 480 kW and 690 kW; on the left) and $\iota_a = 0.34$ (340 kW, 470 kW and 650 kW; on the right) for the W7-AS "standard" configurations (without vertical field). The plasma radius of the discharges at $\iota_a = 0.52$ is defined by the separatrix, $a \simeq 15.5$ cm, and by the small limiter aperture at $\iota_a = 0.34$, $a \simeq 12$ cm (compare with Fig. 4 for full limiter aperture). Thomson scattering data are given by full and the T_e from ECE by open symbols.

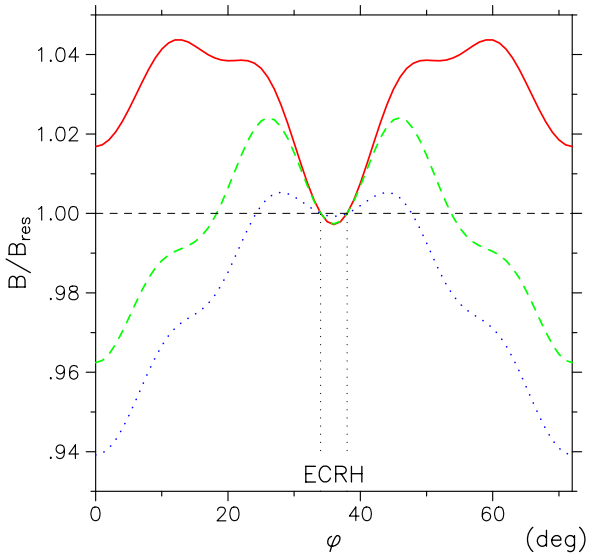

FIG. 2: Magnetic field strength on axis (normalized to B at the ECRH plane) vs. the toroidal angle, φ (for one field period), for $\iota_a = 0.34$ (solid line) and for $\iota_a = 0.52$ (dashed line) without a vertical magnetic field ("standard" configurations). The "maximum-B" configuration with $\iota_a = 0.34$ (dotted line; see Ref. [1]) is given for reference.

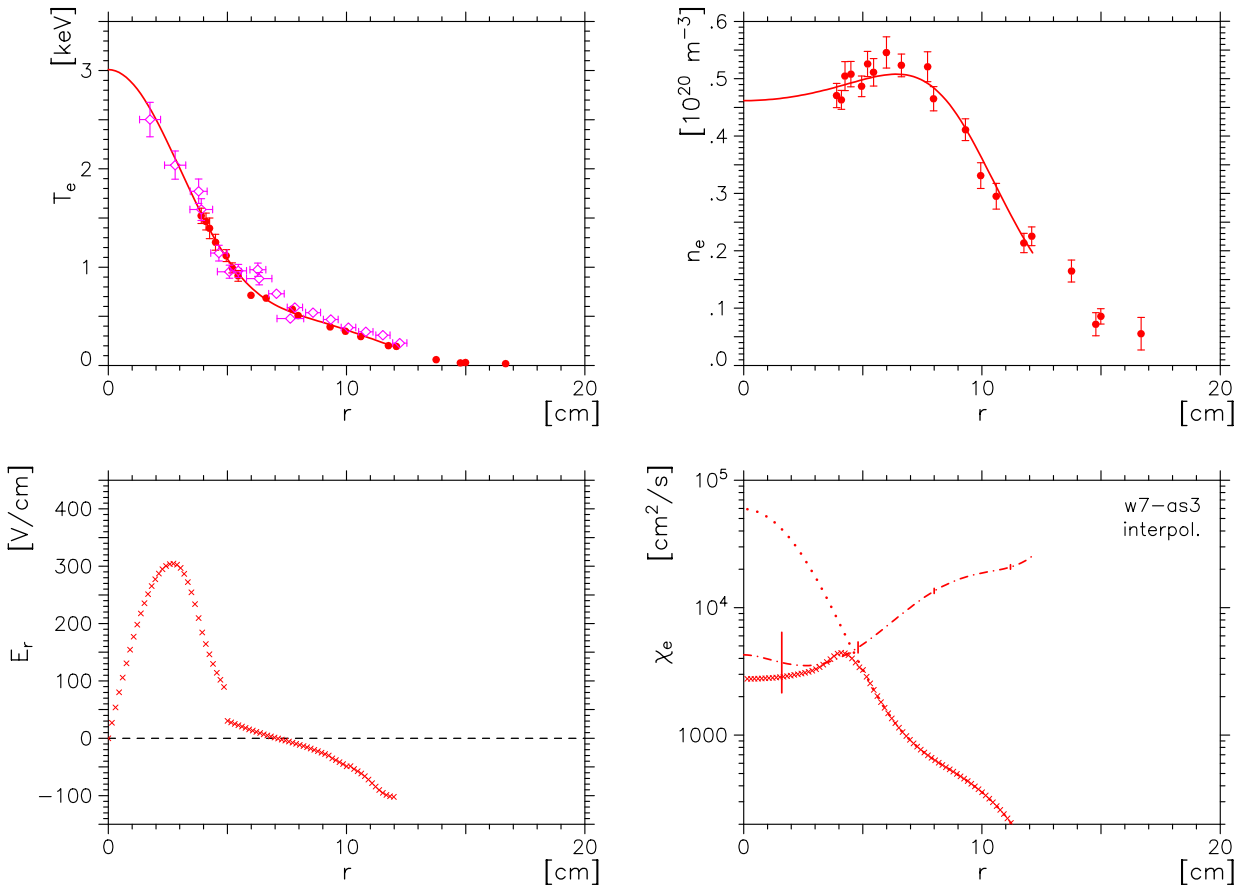

FIG. 3: Neoclassical transport analysis for the discharge of Fig. 1 (on the right) at $t \simeq \frac{1}{3}$ with 650 kW ECRH power: Electron temperature (upper left, full symbols for Thomson scattering and open symbols for ECE data) and density (upper right), ambipolar E_r (lower left) and electron heat diffusivity (lower right plot). The electron heat diffusivity from the energy balance is shown (dot-dashed line with error bars) and compared with the neoclassical predictions obtained with the ambipolar E_r (×, no region of multiple roots in this case) the experimental one (dot-dashed line with error bars), and for the limiting case with $E_r = 0$ (dotted line).

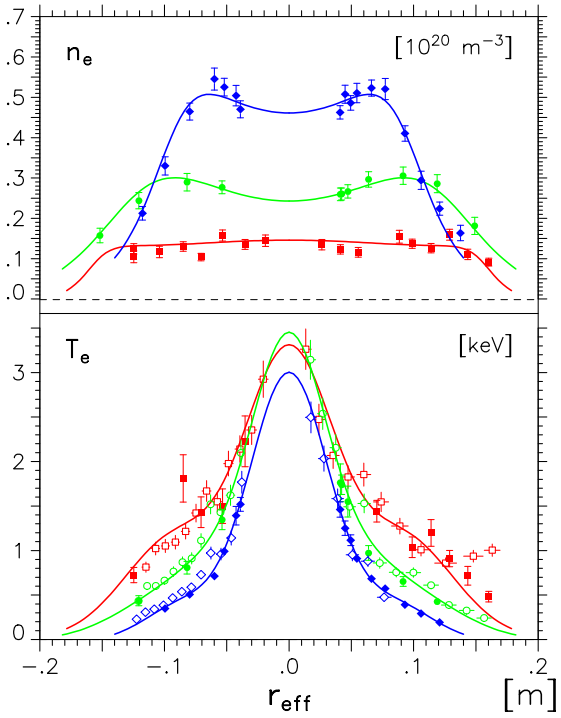

FIG. 4: Density scan (O1-mode) for $\iota \simeq \frac{1}{3}$ with 520 kW (lowest n_e), 640 kW (intermediate n_e) and 650 kW (highest n_e) ECRH power in O1-mode. For the high n_e-discharge, the inserted limiters reduce the plasma radius to 12 cm (about 18 cm for the other discharges); comp. Fig. 1.

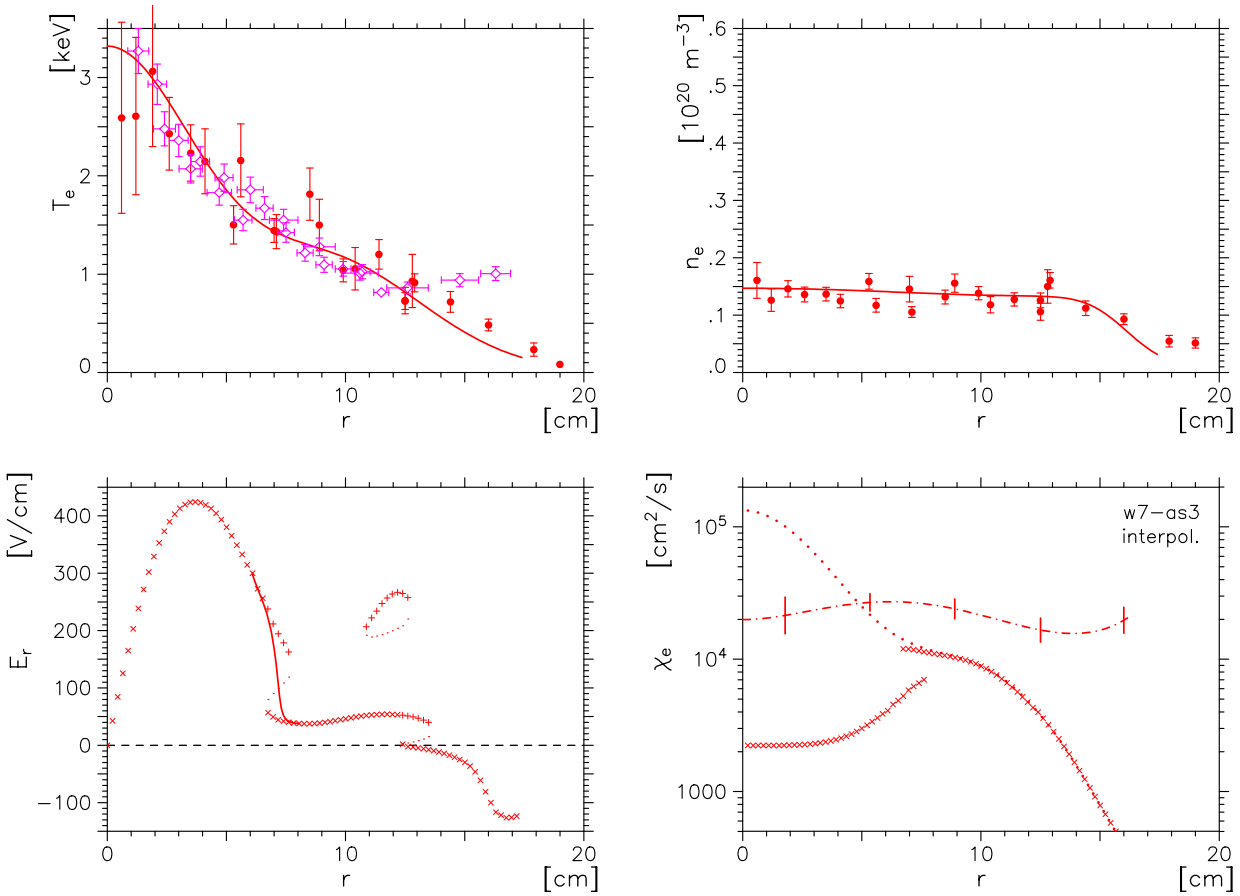

FIG. 5: Neoclassical transport analysis for the low density discharge of Fig. 4 with 520 kW ECRH power; comp. Fig. 3. The E_r within the transition region (solid line) is obtained from the diffusion equation; see [18]. In the region of multiple roots, the neoclassical heat diffusivity is given only for both stable roots.

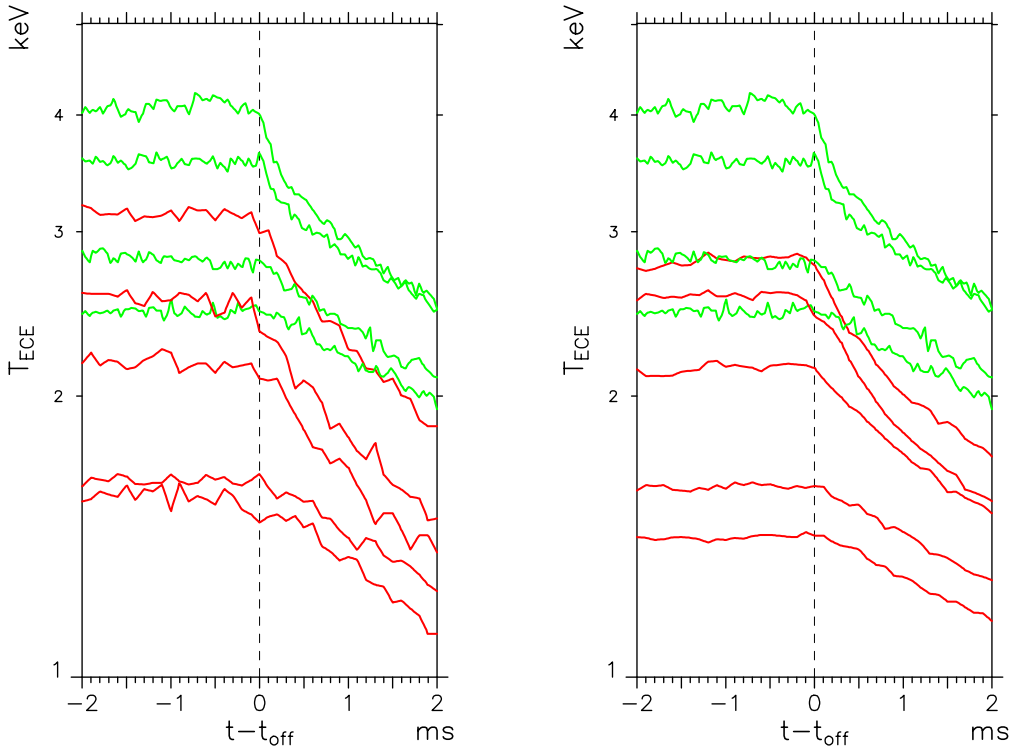

FIG. 6: Time-traces of the electron temperature from ECE for low-τ discharges when the ECRH is switched-off: for the intermediate density in Fig. 4 (on the left) and for the low-n_e (at lower ECRH power as in Fig. 5; on the right). The ECRH X2-mode switch-off phase (with about 800 kW off) is given in both plots for reference (in green/grey); see Fig. 6 in Ref. [1].

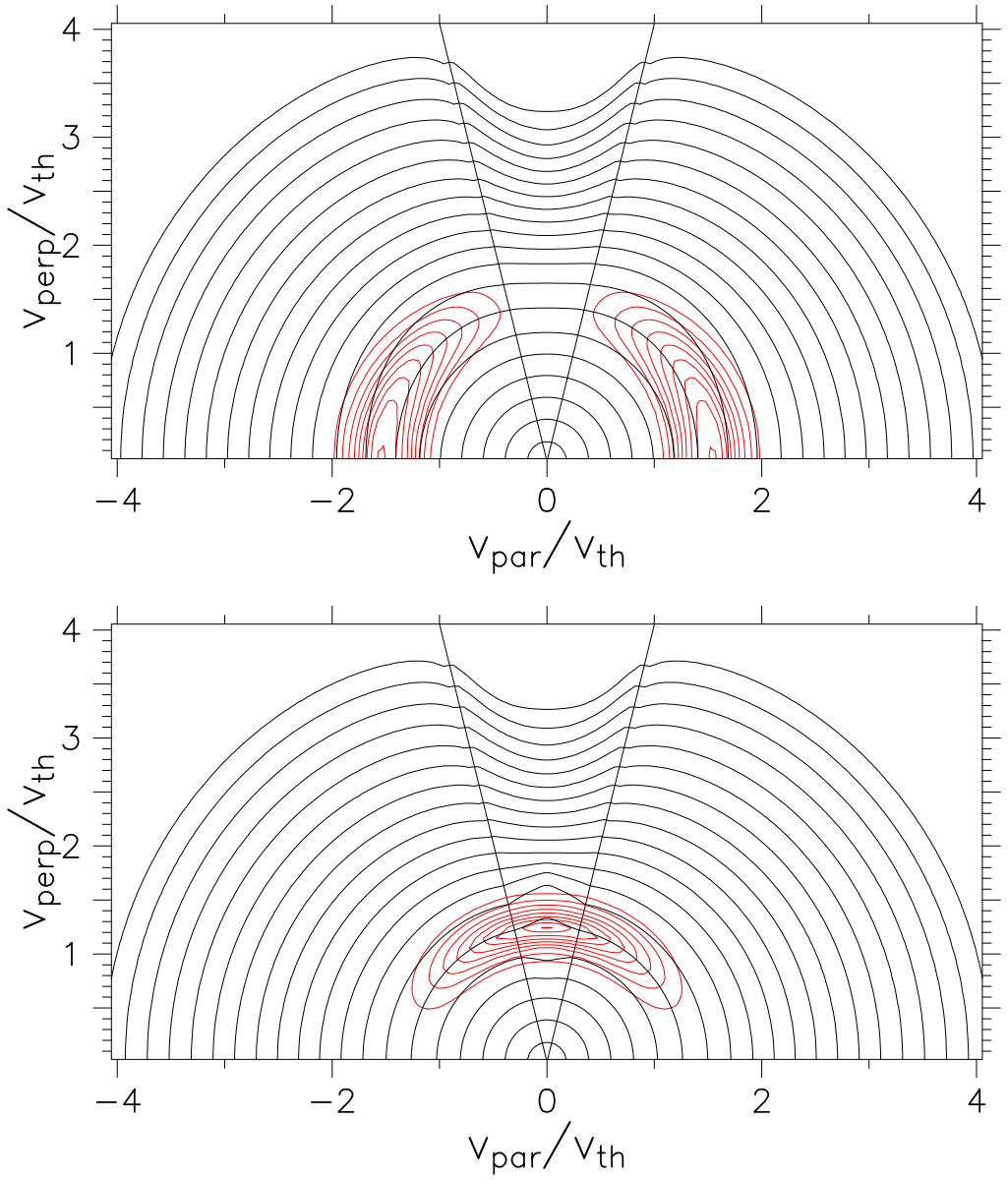

FIG. 7: Isolines of the electron distribution function for ECRH in O1-mode (upper plot) and in X2-mode (lower plot) for the W7-AS "standard" configuration with 30 MW/m^3 power density in linear approach (corresponding to about $r = 0.75$ cm in the ray-tracing calculations). The power sink for balancing the absorbed power is defined only within the loss-cone, $|p| < p_{\rm lc}$ (indicated by the straight lines); see eq. 3. The (averaged) quasi-linear diffusion coefficient, $D_{\perp\perp}$ (eq. 1), calculated from ray-tracing is also given (in red).

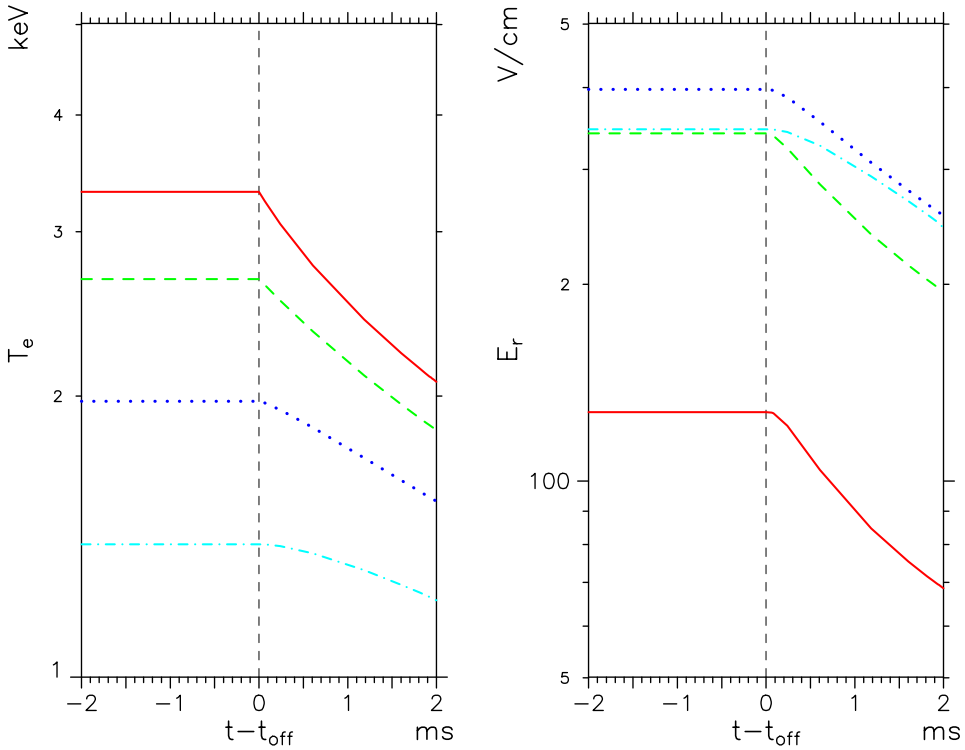

FIG. 8: Time-traces of the electron temperature (on the left) and and of the radial electric field (on the right) calculated with neoclassical diffusion modelling for the low-ι discharges when the ECRH is switched-off; comp. Fig. 6 on the left (intermediate density case). The time-traces for T_e and E_r are given for $r = 0.9,\ 2.7,\ 4.0$ and 5.4 cm (solid, dashed, dotted and dot-dashed line, respectively).